Inverse-Designed Meta-Optics with Spectral-Spatial Engineered Response to Mimic Color Perception

Chris Munley, Wenchao Ma, Johannes E. Fröch, Quentin A. A. Tanguy, Elyas Bayati, Karl F. Böhringer, Zin Lin, Raphaël Pestourie, Steven G. Johnson, and Arka Majumdar*

Meta-optics have rapidly become a major research field within the optics and photonics community, strongly driven by the seemingly limitless opportunities made possible by controlling optical wavefronts through interaction with arrays of sub-wavelength scatterers. As more and more modalities are explored, the design strategies to achieve desired functionalities become increasingly demanding, necessitating more advanced design techniques. Herein, the inverse design approach is utilized to create a set of single-layer meta-optics that simultaneously focus light and shape the spectra of focused light without using any filters. Thus, both spatial and spectral properties of the meta-optics are optimized, resulting in spectra that mimic the color matching functions of the CIE 1931 XYZ color space, which links the spectral distribution of a light source to the color perception of a human eye. Experimental demonstrations of these meta-optics show qualitative agreement with the theoretical predictions and help elucidate the focusing mechanism of these devices.

1. Introduction

Over the recent years, meta-optics have emerged as an elegant solution to control light in both near and far fields, enabling functionalities that would have been perceived as merely theoretically feasible decades back.[1] Their versatile capabilities are enabled by the arrangement of subwavelength scatterers, whose coordinated phase and amplitude response shape the properties of transmitted and/or reflected light fields.[2–6] In the optical domain such sub-wavelength patterns have, for instance, been used to demonstrate lenses,[7–10] polarization control,[11–14] manipulation of light orbital angular momentum,[15–17] spectral filters,[18–20] and structural color prints.[21–23] To achieve these functionalities, forward design approaches are commonly utilized, where intuition or an analytical expression determines the arrangement of scatterers according to their local phase response (e.g., metalenses), or a scatterer geometry is chosen based on a parameter sweep to achieve a wavelength dependent response (e.g., spectral filters). Yet, as this research field grows, requirements on meta-optic functionalities evolve to be progressively stringent as to become suitable for wide-scale practical applications.[24–26] Because with intuitive design approaches such multi-functional meta-optics are very difficult to realize, significant effort has been put forth in the field of computational nanophotonics to identify optimized geometries, leading to the concept of inverse design.[27] For meta-optics, this approach has recently been theoretically explored[28–34] and also used to experimentally demonstrate depth sensing by control of transmitted 3D optical fields,[35] extended depth of focus metalenses in 1D[36] and 2D for full color imaging,[37] polychromatic large-area metalenses,[38] and 3D printed meta-optics.[39] Most of these inverse designs are either used to tailor the spatial focal pattern of meta-optics at discrete wavelengths, or to provide a desired spectral response without any spatial mode engineering. However, for some applications, it would be desirable to simultaneously shape the spectral response and spatial response together, which is not yet reported using inverse design.

Here, we extend the inverse design framework for meta-optics to simultaneously optimize spatial and spectral properties to design single-layer filter-free meta-optics that collect light

C. Munley, J. E. Fröch, A. Majumdar
Department of Physics
University of Washington
Seattle, WA 98195, USA
E-mail: arka@uw.edu

W. Ma
Department of Chemistry
Massachusetts Institute of Technology
Cambridge, MA 02139, USA

J. E. Fröch, Q. A. A. Tanguy, E. Bayati, K. F. Böhringer, A. Majumdar
Department of Electrical and Computer Engineering
University of Washington
Seattle, WA 98195, USA

K. F. Böhringer
Department of Bioengineering
University of Washington
Seattle, WA 98195, USA

K. F. Böhringer
Institute for Nano-Engineered Systems
University of Washington
Seattle, WA 98195, USA

Z. Lin, R. Pestourie, S. G. Johnson
Department of Mathematics
Massachusetts Institute of Technology
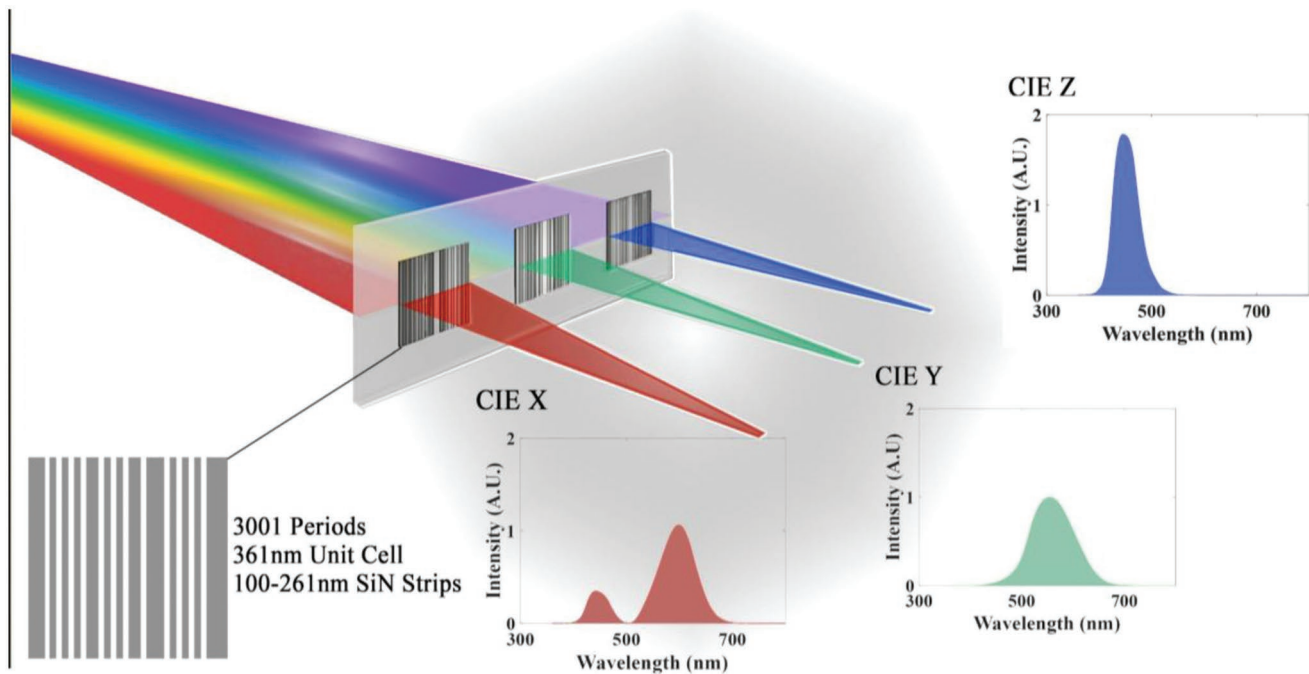Cambridge, MA 02139, USA

Figure 1. Schematic of the CIE XYZ meta-optics. Three separate 1D meta-optics focus light with a spectral response equivalent to the color matching functions of the CIE 1931 XYZ color space from left to right, respectively. The spectral responses are depicted for the respective color space functions.

in a way that mimics the color perception of a human eye. In other words, the functionality that we aim for is focusing a specific spectral distribution to a target area. The spectral distribution is one of the color matching functions of the CIE 1931 XYZ color space,[40] which provides a link between spectra of light and colors perceived by the human eye. In more detail, the color perceived by a human eye is not a physical property of light but is determined by the responses of three types of cone cells in the retina of the eye and how the brain processes and interprets this information.[41] The combined feedback enables the average human to perceive colors of light in the visible spectrum, which roughly ranges from 380 to 740 nm. Thus, to translate spectral measurements to human color experience, device-invariant representations of all colors visible to the average human eye are necessary, and as such the CIE 1931 XYZ color space is often used to validate the color response of displays, assess the effect of pigments on the human eye, and represent the key to relating the objective and subjective natures of color.

Whereas the color perception of a human eye can be described by tristimulus values associated with three color matching functions, we design three meta-optics, each of which corresponds to one of the color matching functions, as schematically depicted in **Figure 1**. These functions follow specific spectral distributions, which distinguish these meta-optics from traditional designs, such as metalenses with hyperbolic phase profiles. Specifically, the shape of the CIE 1931 X function can be approximated by a bimodal distribution, with local maxima near 450 and 600 nm, and an intensity ratio ≈ 1:3. The CIE 1931 Y and Z functions can be approximated with single modes centered near 550 and 450 nm, respectively.[42] However, these two functions strongly differ by the width of the

respective distributions, which are ≈ 100 and 50 nm for the CIE Y and CIE Z functions, respectively.

2. Design

To demonstrate the simultaneous optimization of spectral and spatial properties, we designed 1D meta-optics as schematically shown in Figure 1. Each meta-optic consists of 3001 equally sized cells, each of which contains a silicon nitride stripe on a silica substrate. The length and width of each cell is 1 mm and 361 nm. The stripe width in each cell is used as a design parameter and allowed to vary between 100 and 261 nm. The far field $E_z^{\text{far}}(x, \lambda, w)$ in our specified region can be computed as the convolution of the near field $E_z^{\text{near}}(x', \lambda, w)$ just above the meta-optic and the Green's function $G(x, x', \lambda)$, namely,

$$E_z^{\text{far}}(x, \lambda, w) = \int G(x, x', \lambda) E_z^{\text{near}}(x', \lambda, w) dx' \qquad (1)$$

where x' and x denote spatial coordinates of the near- and far-field regions, with the direction parallel to the metasurface while perpendicular to the stripes; λ denotes the wavelength; and $w = (w_1, w_2, \cdots, w_{3001})$ denotes the widths of the respective bars.

To efficiently simulate the transmitted electric field through such a large-area metasurface composed of periodically arranged subwavelength scatterers, we use a Chebyshev-interpolated surrogate model under a locally periodic approximation (LPA), which allows the field in each unit cell to be computed separately with a periodic boundary condition.[28,34] Because of the subwavelength period, only the transmitted field corresponding to the zeroth-order diffraction contributes
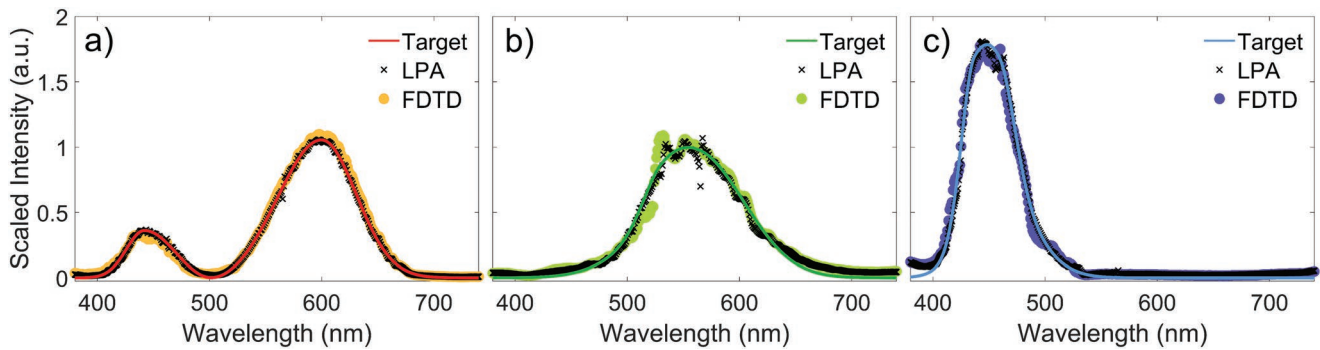
ADVANCED
SCIENCE NEWS

www.advancedsciencenews.com

ADVANCED
OPTICAL
MATERIALS

www.advopticalmat.de

Figure 2. Verification of the optimization based on LPA for the a) CIE X, b) CIE Y, and c) CIE Z meta-optics. The design results under LPA are the first terms in the brackets of Equation (2) multiplied by $f(\lambda_0)/c$.

to the propagating wave. We compute this transmitted electric field in a unit cell for 600 wavelengths at Gauss-Legendre quadrature points and 101 widths of the stripe at Chebyshev nodes using rigorous coupled-wave analysis (RCWA).[32] At each wavelength, the dependence of the field on the width is fitted by Chebyshev interpolation. We thus obtain a surrogate model that quickly evaluates the transmitted electric field near the metasurface.

For each meta-optic, to make the integrated intensity in the specified far-field region A approximate one of the color matching functions, the difference between the engineered spectrum and the target spectrum is minimized, namely, $\min_w$ objective(w), where the objective function can be formulated as

$$\text{objective}(\boldsymbol{w}) = \left\| \frac{\int_A \left| E_z^{far}(x,\lambda,\boldsymbol{w}) \right|^2 dx}{\max_{\boldsymbol{w}} \int_A \left| E_z^{far}(x,\lambda_0,\boldsymbol{w}) \right|^2 dx} - c\frac{f(\lambda)}{f(\lambda_0)} \right\|^2$$

$$= \int_{\lambda_{\min}}^{\lambda_{\max}} \left[\frac{\int_{x_{\min}}^{x_{\max}} \left| E_z^{far}(x,\lambda,\boldsymbol{w}) \right|^2 dx}{\max_{\boldsymbol{w}} \int_{x_{\min}}^{x_{\max}} \left| E_z^{far}(x,\lambda_0,\boldsymbol{w}) \right|^2 dx} - c\frac{f(\lambda)}{f(\lambda_0)} \right]^2 d\lambda \quad (2)$$

Here, $\| \ \|$ denotes the 2-norm of a function of the wavelength λ in $[\lambda_{\min}, \lambda_{\max}] = [380, 740]$ nm; the range of our specified far-field region is $[x_{\min}, x_{\max}] = [-12.5, 12.5]$ μm; $f(\lambda)$ denotes the analytical approximation of one of the color matching functions; c is a dimensionless coefficient that quantifies the tradeoff between maximizing intensity and matching the desired spectrum as explained below; and λ_0 is the peak wavelength of the color matching function, which means $f(\lambda_0) = \max_\lambda f(\lambda)$. The scale factor $\max_{\boldsymbol{w}} \int_A \left| E_z^{far}(x,\lambda_0,\boldsymbol{w}) \right|^2 dx$ is the result of maximizing the integrated intensity at λ_0 over the parameters $\boldsymbol{w}$. This factor, along with $f(\lambda_0)$, nondimensionalizes the objective function and makes the value of c physically meaningful.

While a small value of the objective function and a large intensity in the specified far-field region are preferred, these two goals contradict each other, the tradeoff between which is called the "Pareto front"[43,44] and is quantified by the parameter c. Our objective function would be ideally minimized (to zero) if the integrated intensity were exactly proportional to the desired spectrum $f(\lambda)$ and the intensity at the peak wavelength

λ_0 were equal to the maximized integrated intensity multiplied by c, namely, $c \max_{\boldsymbol{w}} \int_A \left| E_z^{far}(x,\lambda_0,\boldsymbol{w}) \right|^2 dx$. For example, $c = 1$ would mean that we are attempting no tradeoff in intensity at all, that is, trying to both match the spectrum and attain the peak intensity maximized without concern for the spectrum. In practice, a smaller value of c is required in order to achieve good spectral matching (see Section S1, Supporting Information for a comprehensive study of the impact of c on the tradeoff). Our final designs for CIE X, Y, and Z meta-optics correspond to $c = 0.35$, 0.55, and 0.7, respectively, which give good spectral quality with a moderate (30 to 65%) sacrifice in efficiency. The optimized integrated intensity under LPA, the verification using finite-difference time-domain (FDTD) simulation, and the target spectra are compared in **Figure 2**a–c for the CIE X, Y, and Z meta-optics, respectively.

The value of c here can be regarded as a relative focusing efficiency. On the other hand, the absolute focusing efficiency or focusing efficiency can be defined as the ratio between the power transmitted through the specified far-field region and the power of incident light at the peak wavelength. The absolute focusing efficiencies computed with FDTD simulation for the CIE X, Y, and Z meta-optics at the peak wavelengths are 11%, 17%, and 9%, respectively (see Section S2, Supporting Information for the absolute focusing efficiencies at other wavelengths). If we instead maximize the integrated intensity at λ_0 alone, we obtain efficiencies 32%, 32%, and 13%, respectively (consistent with the values of c above). For comparison, in ref. [36], a focusing efficiency of 24.2% at the wavelength $\lambda = 625$ nm is achieved in a smaller 1D metasurface with a diameter of 133 μm, the same materials and a similar geometrical structure as the meta-optics reported here. This efficiency is consistent with our efficiency of 32% when the integrated intensity at $\lambda_0 = 600$ nm is maximized. Our efficiency is higher both because we have a larger aperture and because we are not attempting to focus onto a single diffraction-limited spot. Higher efficiencies can be obtained by 2D metalenses[37] and especially by multilayer structures.[45,46]

The objective function in Equation (2) possesses mirror symmetry in the design parameters (w_1, w_2, ⋯, w_{3001}), that is, the objective function does not change under a mirror reflection of the geometry, that is, $w_i \rightarrow w_{3002-i}$. However, for a nonconvex optimization problem such as the one here, it
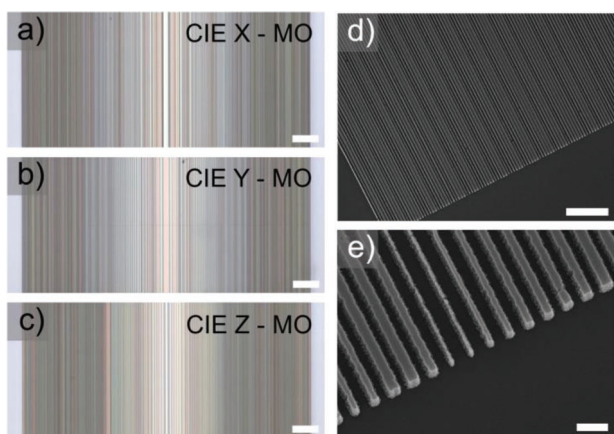
Figure 3. Design and fabrication of the CIE meta-optics (MO). Optical images of the CIE X, Y, and Z meta-optics are shown in (a), (b), and (c), respectively. The scale bars correspond to 100 μm. Magnified SEM images of the Y meta-optic at an oblique angle are shown in (d) and (e). The scale bars in (d) and (e) correspond to 5 μm and 500 nm, respectively.

hard mask deposition, and reactive ion etching. Process parameters and conditions for individual steps are detailed in the Experimental Section. Optical images of the fabricated devices are shown in Figure 3a–c for the CIE X, Y, and Z meta-optics, respectively. Further details of the structures are revealed in scanning electron microscope (SEM) images at an oblique angle in Figure 3d,e, which directly show the successful fabrication of features in the range of 100 to 261 nm for bars with lengths of 1 mm.

3. Results and Discussion

We now turn to the optical characterization of the fabricated devices. Collimated light from a stabilized halogen lamp (Thorlabs SLS302) was transmitted through the sample substrate, then focused by the meta-optic, and was collected using an objective (Nikon Plan Fluor, 40×) with a numerical aperture of 0.75, which exceeds the numerical aperture of the meta-optics (0.3). The collected light was then guided and focused (Thorlabs AC254-30-A; focal length of 30 mm) onto a spectrometer (Princeton Instruments, IsoPlane-320; PIXIS 400B eXcelon), where an adjustable spectrometer slit served as a spatial aperture, limiting the collection area to a confined area in the focal plane.

The experimentally measured spectral dependence on the distance from the design focal plane (1.625 mm) is shown in **Figure 4**a–c for the CIE X, Y, and Z meta-optics, respectively. For comparison, the corresponding simulation data are plotted in Figure 4d–f, where a focal area with the width of 25 μm is assumed. The experimental and simulation results show a good qualitative match in the spectral shifts with
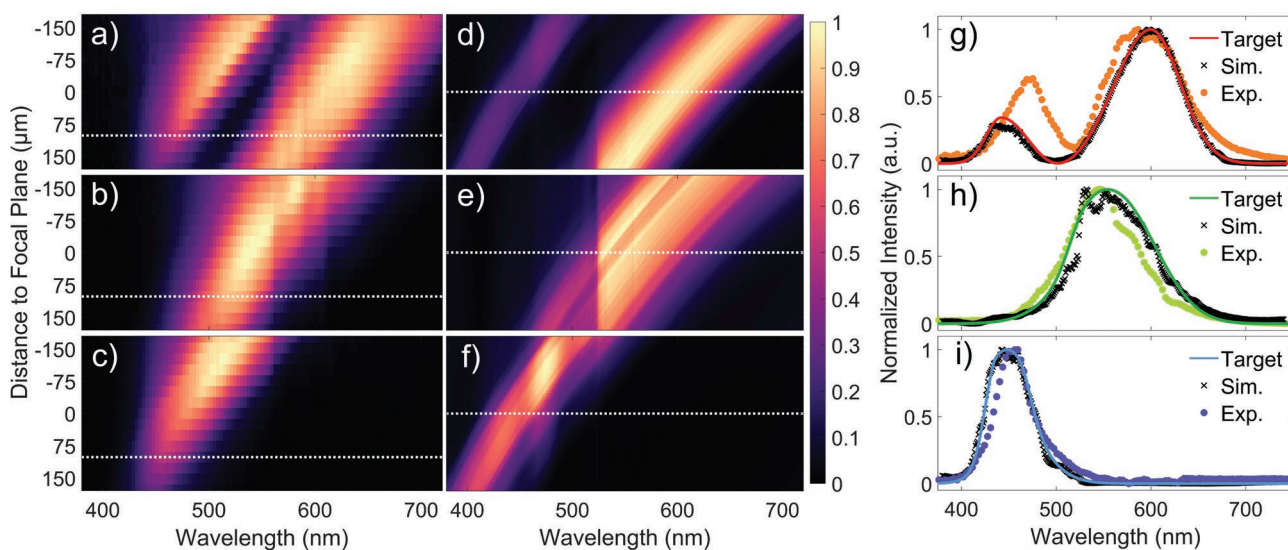
is known that the optimization result can exhibit a spontaneous symmetry breaking, yielding asymmetric optima from symmetric objectives.[47–50] Indeed, we find that our optimized design parameters are asymmetric (as can be seen by looking closely at **Figure 3**). One can also find mirror-symmetrical optima (e.g., by enforcing symmetry during optimization) with similar performance (see Figure S2, Supporting Information).

The optimized designs were then fabricated using a standard nanofabrication approach, in short consisting of deposition of 600 nm SiN on a fused quartz wafer, electron beam lithography,

Figure 4. Spectral response at the focal plane. The spectral response along the optical axis is shown in (a), (b), and (c) for the CIE X, Y, and Z meta-optics, respectively. The vertical coordinate indicates the distance to the design focal plane (1.625 mm). The white lines indicate the distance at which the spectra in (g–i) were collected. Simulated spectra in dependence of the distance to the design focal plane are shown in (d), (e), and (f), for the CIE X, Y, and Z meta-optics, respectively. Experimental (exp.) spectra of the X, Y, and Z meta-optics are compared to simulation (sim.) and to the analytical expression in (g), (h), and (i), respectively. Target spectra are presented as full lines, simulated spectra are presented as crosses, and measured spectra are presented as dots.
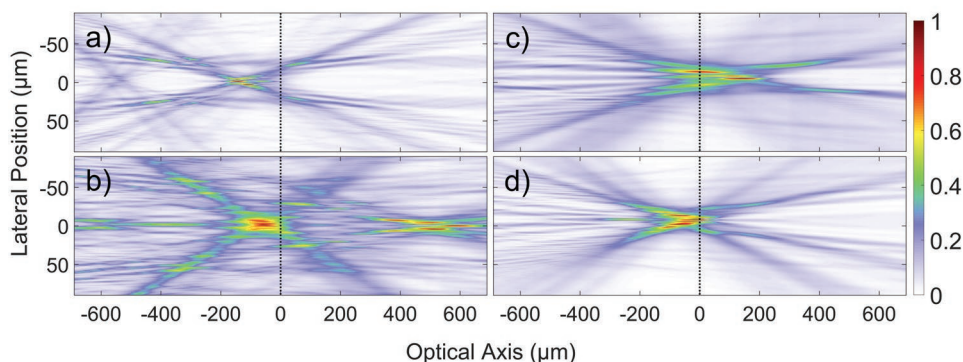
Figure 5. Normalized intensity profiles for transmission of narrowband light sources plotted against the optical axis, relative to the design focal length (indicated by a dashed line). The intensity profiles correspond to a) red and b) blue transmission for the CIE X meta-optic, c) green transmission for the CIE Y meta-optic, and d) blue transmission for the CIE Z meta-optic, respectively.

respect to the distance from the focal plane. The experimental results also exhibit a clear bimodal spectral distribution for the CIE X meta-optic and single modal distributions for the CIE Y and CIE Z meta-optics, which are characteristic of the target spectra. In addition to these agreements, one can note that, in contrast to the simulations, the experimentally collected spectra show a cutoff around 425 nm, below which virtually no intensity was measured. This absence of light is likely related to the spectral distribution of the light source and the system response of the setup (see Section S3, Supporting Information). In the simulation results, one can also observe a demarcation around the wavelength of 523 nm, which is the width of a unit cell (361 nm) multiplied by the refractive index of the substrate (1.45). This feature related to diffraction is not present in the experimental data, probably because of the finite size of the meta-optics along the y direction, which is assumed to be infinite in the simulation. Another apparent difference between simulation and experiment is a systematic redshift of ≈ 25 to 50 nm, which may be related to fabrication imperfections, such as material thickness, or over/under etching.

To demonstrate that the targeted functionality is achievable, we make a comparison of the desired CIE color matching functions, simulations, and spectra measured at a fixed distance (100 μm) from the design focal plane, as presented in Figure 4g–i for the CIE X, Y, and Z meta-optics, respectively. The comparison shows a qualitative match between the target spectra and the experimental results. We emphasize here that the inverse design proves successful as we simultaneously achieve focusing and spectral engineering, as evidenced by: a close spectral match in the proximity of the target focal plane for all three devices; distinct spectral features, such as the bimodal distribution of the transmitted light for the CIE X meta-optic with a node near 500 nm while maintaining the relative intensity distribution of the target spectra; and the characteristic spectral widths that, in all three cases, follow the trends of the target spectra. Particularly, the CIE Y meta-optic displays the broadest spectral distribution with a full width half maximum (FWHM) of ≈ 100 nm, while a narrower spectrum was observed for the CIE Z meta-optic with a FWHM of ≈ 50 nm, as intended. To quantify the deviation from the target spectra

we calculated the root mean square error (RMSE) between target and simulation, as well as between target and experimentally measured values, defined as $\text{RMSE} = \sqrt{\dfrac{\sum_{i=1}^{N}(x_i - \hat{x}_i)^2}{N}}$, where N is the number of data points in the spectrum, x_i is the measured/simulated intensity at data point i, and $\hat{x}_i$ is the corresponding value of the CIE target function, normalized so that the maximum of the target spectra is 1. For the simulated spectra we obtained RMSE values of 0.01, 0.05, and 0.02 for the CIE X, Y, and Z functions, whereas for the experimentally measured spectra we obtained values of 0.15, 0.11, and 0.08.

Because the inverse design process is non-intuitive, the emergence of complex spectral features requires further characterization. To unravel the underlying focusing mechanism we measure the lateral intensity profiles along the optical axis for transmitted light with defined spectral bands at (635 ± 6) nm, (530 ± 16) nm, and (455 ± 9) nm, from which we reconstruct a red (R), green (G), and blue (B) response (further detailed in the Experimental Section).

The essential features of the intensity profiles are summarized in **Figure 5**a,b for the R and B responses of the CIE X meta-optic, respectively, while Figure 5c shows the G response of the CIE Y meta-optic, and Figure 5d displays the B response of the CIE Z meta-optic, with the full intensity profiles presented in the Section S5, Supporting Information. For the R and B response of the CIE X meta-optic, we identify two major focal spots, which are separated by ≈ 500 μm along the optical axis. The first focal spot of B is closely situated to the focal spot of R, while at the same time a lower field intensity can be assumed for wavelengths between G and B, due to the separation along the optical axis of the wavelength dependent focal spots, which thus results in the bimodal shape of the target spectrum at the focal plane. Next, the CIE Y and Z meta-optics both possess one distinct focal spot, resulting in a spectral response with a unimodal distribution at the design focal plane. The main difference arises in the apparent focusing efficiency. The CIE Z meta-optic has a tighter focal spot for B in the focal plane as well as along the optical axis, whereas the focal spot of the CIE Y meta-optic is slightly extended in the focal plane and along the optical axis. As the focal spot is extended, the

**ADVANCED
SCIENCE NEWS**

www.advancedsciencenews.com

**ADVANCED
OPTICAL
MATERIALS**

www.advopticalmat.de

width of the spectral distribution also becomes extended, as the extended depth-of-field for the CIE Y meta-optic as compared to the CIE Z meta-optic leads to a relatively broader spectrum at the focal plane. Comprehensively, these distinct features underlie the non-trivial focusing behavior of the CIE X, Y, and Z meta-optics, distinguishing them from traditional designs, such as the hyperbolic metalens. In addition, we have simulated the intensity profiles for transmitted light with the same spectral distributions as the R, G, and B sources. As presented in Section S6, Supporting Information, the experimentally observed profiles match with their specific features with the simulated profiles.

4. Conclusion

In summary, we have designed a set of single-layer filter-free 1D meta-optics with 1 mm width. These meta-optics focus transmitted light to a specified area in the focal plane with a spectral response mimicking the CIE 1931 XYZ color matching functions. The measured spectral responses show qualitative agreement with the targets. Some key features of the target spectra, such as the bimodal spectral distribution and the full widths at half maxima, are reproduced experimentally. We have also studied the focusing mechanism of the meta-optics from the spatial intensity profiles. Although some fabrication imperfections seem to currently limit the device performance, further improvement in the fabrication process, as well as development in the design method by considering the robustness of the design process could further improve the spectral matching to the target design.

Nevertheless, through our work, we have demonstrated the capability to create devices that bridge the gap between the spectral distribution of a light source and human color perception. We have thus combined the capabilities of focusing light with distinct broad spectral distributions that span the visible range. While in our case three different meta-optics are used, these could be incorporated into the same device with at least three sensors, which could measure the relative magnitude of the tristimulus values. Beyond our work, such meta-optics may be applicable in the future as elements to assist in color sensing and in general pave the way for devices with more complex functionalities.

5. Experimental Section

Simulations: The framework of optimization, as reviewed above, was similar to those in refs. [28,34,36]. The transmitted electric field in a unit cell under periodic boundary conditions was computed using RCWA implemented in a free and open-source software package.[32] A surrogate model maps the width of the stripe in a unit cell to transmitted electric field based on Chebyshev interpolation.[51] The convolution between the near field and the Green's function was performed by fast Fourier transforms.[52] The objective function in Equation (2) was based on the integrated intensity in the specified far-field region. This integrated intensity was roughly proportional to the transmission power computed from the Poynting vector. The objective function can also be formulated in terms of the transmission power, but the computational cost will be increased. The nonlinear optimization was performed by the CCSA-MMA algorithm[53] implemented in a free and open-source software package.[51] For each meta-optic, two such optimization tasks were involved. The first optimization was to maximize the integrated intensity in the specified far-field region at the peak wavelength, which typically takes a few minutes. The second optimization was to minimize the objective function in Equation (2). The optimizations with different values of c were performed in parallel, and the time cost of each optimization on a single CPU was on the order of 10 h. The final designs of the meta-optics were validated by FDTD simulation also using a free and open-source software package.[54] (RWCA was not suitable for this verification because it was designed for periodic structures while the reported meta-optics here were not periodic.)

Fabrication: All devices were fabricated using the following fabrication process. First, a 600 nm SiN film was deposited on quartz using plasma enhanced chemical vapor deposition (SPTS Delta LPX PECVD). A positive polymer resist (ZEP 520) was spin coated, followed by deposition of a thin Au/Pd layer for charge dissipation. Electron beam lithography (JEOL JBX6300FS, 100 kV, 1 nA) was used to write the meta-optics layout in the resist. After exposure, the Au/Pd layer was removed using TFA gold etchant and the resist was developed in amyl acetate for 2 min. Then an AlO_x layer ($\approx$ 60 nm) was deposited in a thermal evaporator, followed by resist lift-off by ultrasonication in dichloromethane. The AlO_x layer served as a hard mask in the following reactive ion etching step (Oxford Plasma Lab 100, ICP-180), where the SiN film was etched entirely. Finally, the devices were cleaned in a benign O_2 plasma.

Optical Characterization: The presented spectra were based on the experimentally recorded spectra corrected by background (i.e., light not diffracted by the meta-optic) and the spectral distribution of the light source (see Section S2, Supporting Information).

For measurements of the field profile in transmission, the sample was mounted at a fixed position, and a microscope assembly consisting of an objective (Nikon Plan Fluor 20×, 0.5 NA), tube lens (Thorlabs, focal length of 200 mm), and CMOS camera (Allied Vision ProSilica GT1930C) were aligned on a translation stage (NewPort ILS100CC). The position of the assembly was then swept in a range from 0 up to 3 mm with respect to the sample surface, while the lateral transmission intensity was captured in the objective focal plane for consecutive runs of the R, G, and B light sources.

Supporting Information

Supporting Information is available from the Wiley Online Library or from the author.

Conflict of Interest

The authors declare no conflict of interest.

Data Availability Statement

The data that support the findings of this study are available from the corresponding author upon reasonable request.

Keywords

[1] C. L. Holloway, E. F. Kuester, J. A. Gordon, J. O'Hara, J. Booth, D. R. Smith, *IEEE Antennas Propag. Mag.* **2012**, *54*, 10.

[2] W. T. Chen, A. Y. Zhu, F. Capasso, *Nat. Rev. Mater.* **2020**, *5*, 604.

[3] H.-H. Hsiao, C. H. Chu, D. P. Tsai, *Small Methods* **2017**, *1*, 1600064.

[4] D. Neshev, I. Aharonovich, *Light: Sci. Appl.* **2018**, *7*, 58.

[5] S. M. Kamali, E. Arbabi, A. Arbabi, A. Faraon, *Nanophotonics* **2018**, *7*, 1041.

[6] S. Colburn, A. Zhan, E. Bayati, J. Whitehead, A. Ryou, L. Huang, A. Majumdar, *Opt. Mater. Express* **2018**, *8*, 2330.

[7] A. Arbabi, Y. Horie, A. J. Ball, M. Bagheri, A. Faraon, *Nat. Commun.* **2015**, *6*, 7069.

[8] A. Zhan, S. Colburn, R. Trivedi, T. K. Fryett, C. M. Dodson, A. Majumdar, *ACS Photonics* **2016**, *3*, 209.

[9] R. Paniagua-Domínguez, Y. F. Yu, E. Khaidarov, S. Choi, V. Leong, R. M. Bakker, X. Liang, Y. H. Fu, V. Valuckas, L. A. Krivitsky, A. I. Kuznetsov, *Nano Lett.* **2018**, *18*, 2124.

[10] M. Khorasaninejad, W. T. Chen, R. C. Devlin, J. Oh, A. Y. Zhu, F. Capasso, *Science* **2016**, *352*, 1190.

[11] Y. Intaravanne, X. Chen, *Nanophotonics* **2020**, *9*, 1003.

[12] M. Khorasaninejad, K. B. Crozier, *Nat. Commun.* **2014**, *5*, 5386.

[13] M. Khorasaninejad, W. T. Chen, A. Y. Zhu, J. Oh, R. C. Devlin, D. Rousso, F. Capasso, *Nano Lett.* **2016**, *16*, 4595.

[14] L. Carletti, A. Zilli, F. Moia, A. Toma, M. Finazzi, C. De Angelis, D. N. Neshev, M. Celebrano, *ACS Photonics* **2021**, *8*, 731.

[15] K. E. Chong, I. Staude, A. James, J. Dominguez, S. Liu, S. Campione, G. S. Subramania, T. S. Luk, M. Decker, D. N. Neshev, I. Brener, Y. S. Kivshar, *Nano Lett.* **2015**, *15*, 5369.

[16] X. Fang, H. Ren, M. Gu, *Nat. Photonics* **2020**, *14*, 102.

[17] H. Ren, S. A. Maier, *Adv. Mater.* **2021**, https://doi.org/10.1002/adma.202106692.

[18] C.-S. Park, V. R. Shrestha, W. Yue, S. Gao, S.-S. Lee, E.-S. Kim, D.-Y. Choi, *Sci. Rep.* **2017**, *7*, 2556.

[19] Y. Horie, A. Arbabi, E. Arbabi, S. M. Kamali, A. Faraon, *Opt. Express* **2016**, *24*, 11677.

[20] M. Faraji-Dana, E. Arbabi, A. Arbabi, S. M. Kamali, H. Kwon, A. Faraon, *Nat. Commun.* **2018**, *9*, 4196.

[21] F. Cheng, J. Gao, T. S. Luk, X. Yang, *Sci. Rep.* **2015**, *5*, 11045.

[22] W. Yang, S. Xiao, Q. Song, Y. Liu, Y. Wu, S. Wang, J. Yu, J. Han, D.-P. Tsai, *Nat. Commun.* **2020**, *11*, 1864.

[23] K. Seo, M. Wober, P. Steinvurzel, E. Schonbrun, Y. Dan, T. Ellenbogen, K. B. Crozier, *Nano Lett.* **2011**, *11*, 1851.

[24] J. Scheuer, *ACS Photonics* **2020**, *7*, 1323.

[25] C.-W. Qiu, T. Zhang, G. Hu, Y. Kivshar, *Nano Lett.* **2021**, *21*, 5461.

[26] L. Huang, S. Colburn, A. Zhan, A. Majumdar, *Adv. Photonics Res.* **2022**, *3*, 2100265.

[27] S. Molesky, Z. Lin, A. Y. Piggott, W. Jin, J. Vucković, A. W. Rodriguez, *Nat. Photonics* **2018**, *12*, 659.

[28] R. Pestourie, C. Pérez-Arancibia, Z. Lin, W. Shin, F. Capasso, S. G. Johnson, *Opt. Express* **2018**, *26*, 33732.

[29] Z. Lin, B. Groever, F. Capasso, A. W. Rodriguez, M. Lončar, *Phys. Rev. Appl.* **2018**, *9*, 044030.

[30] H. Chung, O. D. Miller, *ACS Photonics* **2020**, *7*, 2236.

[31] H. Chung, H. Chung, O. D. Miller, O. D. Miller, *Opt. Express* **2020**, *28*, 6945.

[32] W. Jin, W. Li, M. Orenstein, S. Fan, *ACS Photonics* **2020**, *7*, 2350.

[33] Z. Lin, C. Roques-Carmes, R. Pestourie, M. Soljačić, A. Majumdar, S. G. Johnson, *Nanophotonics* **2021**, *10*, 1177.

[34] Z. Lin, R. Pestourie, C. Roques-Carmes, Z. Li, F. Capasso, M. Soljačić, S. G. Johnson, *arXiv:2111.01071v1* **2021**.

[35] A. Zhan, R. Gibson, J. Whitehead, E. Smith, J. R. Hendrickson, A. Majumdar, *Sci. Adv.* **2019**, *5*, eaax4769.

[36] E. Bayati, R. Pestourie, S. Colburn, Z. Lin, S. G. Johnson, A. Majumdar, *ACS Photonics* **2020**, *7*, 873.

[37] E. Bayati, R. Pestourie, S. Colburn, Z. Lin, S. G. Johnson, A. Majumdar, *Nanophotonics* **2021**, *11*, 2531.

[38] Z. Li, R. Pestourie, J.-S. Park, Y.-W. Huang, S. G. Johnson, F. Capasso, *arXiv:2104.09702* **2021**.

[39] C. Roques-Carmes, Z. Lin, R. E. Christiansen, Y. Salamin, S. E. Kooi, J. D. Joannopoulos, S. G. Johnson, M. Soljačić, *ACS Photonics* **2022**, *9*, 43.

[40] T. Smith, J. Guild, *Trans. Opt. Soc.* **1931**, *33*, 73.

[41] C. F. Bohren, E. E. Clothiaux, in *Fundamentals of Atmospheric Radiation*, Wiley, New York **2006**, pp. 185–239.

[42] C. Wyman, P.-P. Sloan, P. Shirley, *J. Comput. Graphics Tech.* **2013**, *2*, 1e11.

[43] A. Jahan, K. L. Edwards, M. Bahraminasab, *Multi-Criteria Decision Analysis for Supporting the Selection of Engineering Materials in Product Design*, Butterworth-Heinemann, Oxford **2016**.

[44] R. T. Marler, J. S. Arora, *Struct. Multidiscip. Optim.* **2010**, *41*, 853.

[45] Z. Lin, C. Roques-Carmes, R. E. Christiansen, M. Soljačić, S. G. Johnson, *Appl. Phys. Lett.* **2021**, *118*, 041104.

[46] R. E. Christiansen, R. E. Christiansen, R. E. Christiansen, Z. Lin, C. Roques-Carmes, Y. Salamin, S. E. Kooi, J. D. Joannopoulos, J. D. Joannopoulos, M. Soljačić, M. Soljačić, S. G. Johnson, S. G. Johnson, *Opt. Express* **2020**, *28*, 33854.

[47] J. P. Boyd, *Chebyshev & Fourier Spectral Methods*, 2nd ed., Dover Publication, New York **2000**.

[48] X. Guo, C. Ni, G. Cheng, Z. Du, *Struct. Multidiscip. Optim.* **2012**, *46*, 631.

[49] J. N. Richardson, S. Adriaenssens, P. Bouillard, R. F. Coelho, *Struct. Multidiscip. Optim.* **2013**, *47*, 631.

[50] Y. Zhang, Q. Qu, J. Wright, *arXiv:2007.06753* **2021**.

[51] S. G. Johnson, *FastChebInterp*, https://github.com/stevengj/FastChebInterp.jl (accessed: July 2021).

[52] M. Frigo, S. G. Johnson, in *Proceedings of the 1998 IEEE International Conference on Acoustics, Speech and Signal Processing*, Vol. *3*, IEEE, Piscataway, NJ **1998**, pp. 1381–1384.

[53] K. Svanberg, *SIAM J. Optim.* **2006**, *12*, 555.

[54] A. F. Oskooi, D. Roundy, M. Ibanescu, P. Bermel, J. D. Joannopoulos, S. G. Johnson, *Comput. Phys. Commun.* **2010**, *181*, 687.